Neurological mechanism of sensory deficits after developmental exposure to non-dioxin-like polychlorinated biphenyls (PCBs)

Nadja R. Brun[1], Jennifer M. Panlilio[1], Kun Zhang[2,3], Yanbin Zhao[2,3], Evgeny Ivashkin[4,5], John J. Stegeman[1], Jared V. Goldstone[1]

[1] Department of Biology, Woods Hole Oceanographic Institution, Woods Hole, MA, USA
[2] School of Environmental Science and Engineering, Shanghai Jiao Tong University, 800 Dongchuan Road, Shanghai 200240, China
[3] Shanghai Institute of Pollution Control and Ecological Security, Shanghai 200092, China
[4] Josephine Bay Paul Center for Comparative Molecular Biology and Evolution, Marine Biological Laboratory, Woods Hole, MA, USA
[5] A.N. Severtsov Institute of Ecology and Evolution, Russian Academy of Sciences, Moscow, Russia

Address correspondence to
Nadja Brun, nbrun@whoi.edu

Woods Hole Oceanographic Institution, Mail Stop 32
266 Woods Hole Road
Woods Hole, MA 02543

Competing Financial Interests

The authors declare they have no actual or potential competing financial interests.

Abstract

The most abundant polychlorinated biphenyl (PCB) congeners found in the environment and in humans are neurotoxic. This is of particular concern for early life stages because the exposure of the more vulnerable developing nervous system to chemicals can result in neurobehavioral disorders. To uncover currently unknown links between PCB target mechanisms and neurobehavioral deficits, we investigated the effects of the non-dioxin-like (NDL) congener PCB153 on neuronal morphology and synaptic transmission linked to the proper execution of a sensorimotor response using zebrafish as a vertebrate model. Zebrafish that were exposed during development to concentrations similar to those found in human cord blood and PCB contaminated sites showed a delay in startle response. A similar delay was observed for other NDL congeners but not for the potent dioxin-like congener PCB126. Morphological and biochemical data demonstrate that while exposure to PCB153 induced swelling of afferent sensory neurons, the disruption of dopaminergic and GABAergic signaling is the dominant mechanism associated with motor movement. The effects on important and broadly conserved signaling mechanisms in vertebrates suggest that NDL PCBs may contribute to neurodevelopmental abnormalities in humans and, with the startle response being critical for the survival of fish, to evolutionary adaptation in wildlife.

Introduction

Humans and wildlife are exposed to a wide range of contaminants in the environment and the role of these chemical pollutants in developmental neurotoxicity, cognitive impairment, and neurodegenerative disorders has become a global environmental health concern (Landrigan et al. 2018). Among the top industrial-derived contaminants thought to be involved in developmental neurotoxicity are polychlorinated biphenyls (PCBs) (Boix et al. 2010; Boucher et al. 2009; Grandjean and Landrigan 2014). For decades, PCBs have been used as insulators, coatings, and caulks, and have persisted to date in the environment where they have globally accumulated in wildlife tissue and human cord blood, amniotic fluid, and mother's milk (Ennaceur et al. 2008; Lancz et al. 2015a). PCBs are comprised of planar, dioxin-like (DL) congeners that lack ortho-chlorine substituents as well as non-planar, non-dioxin-like (NDL) congeners which have ortho-chlorine substituents. The levels of NDL PCBs in human and environmental samples are far greater than the levels of DL congeners, with NDL PCB153 and PCB138 being generally the most abundant. In human cord blood, PCB153 concentrations range from 3.7 to 200 ng g^{-1} lipid (Bergonzi et al. 2009; Herbstman et al. 2007; Lancz et al. 2015b; Patel et al. 2018).

During the early stages of life, the nervous system is generally more sensitive to chemical exposure compared to fully developed adults (Rice and Barone 2000), and therefore it is essential to identify the neurotoxic mechanisms that underpin the behavioral effects of environmental exposure to different PCBs during gestation and early life stages if we want to successfully treat and remediate health effects in humans and wildlife. Early developmental exposure to PCBs is associated with many neurodevelopmental disorders. For instance, increased serum PCB concentrations in children are associated with deficits in cochlear functions (Jusko et al. 2014; Trnovec et al. 2010), fine motor skills (Ribas-Fitó et al. 2001; Walkowiak et al. 2001), and cognitive impairment (Boucher et al. 2009; Chen et al. 1992). In rats, developmental exposure to NDL PCBs has been linked to behavioral changes, including hyperactivity, impulsiveness, and impairment of cognitive function (Berger et al.

66 2001; Boix et al. 2010; Johansen et al. 2014). NDL PCB developmental exposure also
67 adversely affect the auditory function in adult rats, including elevated thresholds of brainstem
68 auditory evoked potentials, auditory deficits at low frequencies, audiogenic seizures, and
69 reduced auditory startle responses (Crofton et al. 2000; Goldey et al. 1995; Lilienthal et al.
70 2011, 2015; Poon et al. 2015). The observed effect on the auditory-evoked startle response
71 is particularly relevant as it plays a critical role in the performance and survival of fish and
72 amphibians, and involves cellular functions, sensory-motor pathways, and monoamine
73 neurotransmitters that, ranging from fish to humans, are conserved among vertebrates
74 (Stewart et al. 2014).

75 To date, mechanistic studies of neurodevelopmental effects of NDL PCBs suggest three
76 major targets: (1) alterations in neurotransmission, particularly involving dopamine and
77 serotonin, and consequently disruptions to Ca^{2+} signal transduction (Campagna et al. 2011;
78 Dervola et al. 2015; Enayah et al. 2018; Fonnum and Mariussen 2009; Langeveld et al.
79 2012), (2) loss of outer hair cells (Crofton et al. 2000; Trnovec et al. 2010), and (3) altered
80 axonal or dendritic morphogenesis (Keil et al. 2019; Lein et al. 2007; Pruitt et al. 1999; Yang
81 et al. 2009). The links between these PCB targets and neurobehavioral deficits remain
82 unknown. We used the zebrafish auditory system (**Figure 1**) as a model to decipher the
83 involvement of these three major targets in disrupting the startle response after
84 developmental exposure to NDL PCB153. Many of the pathways and genes that regulate
85 startle behavior in fish also operate in human neurological disorders (Howe et al. 2013;
86 Maximino and Herculano 2010; Meserve et al. 2020; Tropepe and Sive 2003; Wolman et al.
87 2015). We demonstrate that environmentally relevant concentrations (10 nM) of NDL
88 PCB153 alter startle response which coincided with axonal swelling and dysregulated
89 dopamine metabolite and GABA levels. Co-exposures to the dopamine D2-receptor
90 antagonist and GABA receptor modulator drug haloperidol alleviated the delay in startle
91 response. While similar responses were observed for other di-*ortho* NDL PCBs and the
92 mono-*ortho* congener PCB118, a delayed startle response was not observed with the non-

93 *ortho* PCB126, a potent AHR agonist. These results highlight the potential of low
94 concentrations of NDL PCBs to disrupt broadly conserved neurotransmission tied to a
95 mechanosensory deficit.

96 # Results

97 **Morphological Effects**

98 Exposure to contaminants during development can result in reduced growth, which can
99 affect kinematics in swimming behavior (Voesenek et al. 2018). Zebrafish larvae exposed to
100 1000 nM PCB153 developed normally with no difference in body length at 6 dpf in
101 comparison to the control group, in three separate trials (Trial 1: $t(25.98) = .661$, $p = .514$;
102 Trial 2: $t(37.98) = .443$, $p = .660$; Trial 3: $t(37.43) = .645$, $p = .523$; **Figure S1, Supplemental**
103 **Material**).

104 **Behavioral effects**

105 Rohon-Beard cells are mechanosensory neurons that appear earliest during development in
106 zebrafish. They are located in the dorsal region of the embryonic spinal cord and appear
107 around 24 hpf (Roberts 2000). A few days into development, Rohon-Beard cells also relay
108 sensory information to the M-cells (Liu and Hale 2017). In our experiments, a tactile stimulus
109 on the trunk at 26 hpf evoked a C-shaped body flexion in both the DMSO- and the 1000 nM
110 PCB153-treated embryos ($U = 183$, $p = .599$; **Figure S2**), indicating that the formation and
111 function of Rohon-Beard cells were not impaired by PCB153.

112 Spontaneous and light-dark-stimulated swimming activity assessed at 6 dpf revealed that
113 larvae exposed to PCB153 (1000 nM) had lower cumulative locomotion activity over ten
114 minutes ($M = 1182$ mm, $SD = 382$) in comparison to the control group ($M = 1510$ mm, $SD =$
115 402), $t(132.4) = 4.854$, $p < .0001$ (**Figure S3A**). Zebrafish larvae typically increase
116 locomotion in dark conditions following light exposure. Once stimulated by a rapid loss of
117 illumination, both treatment groups exhibited similar swimming activity (**Figure S3B**).

118 The vibro-acoustic startle response includes two distinct motor behaviors: a short-latency C-
119 bend (SLC**)** initiated within 5-15 ms of the stimulus, or a long-latency C-bend (LLC)
120 beginning from 15-100 ms after the stimulus (Burgess and Granato 2007). The mean latency
121 value calculated as the average of all SLC and LLC responses in each treatment population
122 was 21 ± 20 ms for control larvae at the highest vibro-acoustic stimulus intensity (**Figure 2A,**
123 **2B**). By contrast, the NDL PCB-treated larvae that responded to the stimulus showed
124 significantly longer average latencies in response to the same stimulus intensity given the
125 controls, $H(8) = 368.6$, $p < .0001$. Larvae exposed to PCB153 responded at mean latencies
126 that increased with dose. Thus at 10 nM PCB153 the latency was 26 ± 27 ms, at 30 nM it
127 was 50 ± 36 ms, at 100 nM it was 50 ± 30 ms, and at 1000 nM the latency was 68 ± 32 ms.
128 Results with the lowest PCB153 concentration tested (10 nM) were not significantly different
129 from controls ($p = .752$). Larvae exposed to other NDL congeners also showed long
130 latencies; with PCB138 it was 52 ± 37 ms, with PCB118 it was 45 ± 27 ms, and with PCB52
131 it was 39 ± 32 ms. Unlike the NDL PCB-treated larvae, larvae treated with the potent DL
132 PCB126 had a mean latency of 22 ± 22 ms, essentially identical to that in the controls ($p =$
133 $.999$).

134 Examining the SLC and the LLC responses separately can give insight into the underlying
135 mechanism of effect. A greater stimulus intensity increases the probability of evoking an
136 SLC, shifting the response bias from LLC to SLC (Troconis et al. 2017). Consistent with that
137 we observed a shift to SLC with increasing stimulus intensity in solvent control (DMSO-
138 treated) larvae (**Figure 2C, Figure S4A**). Larvae were tested 4 times at each stimulus
139 intensity. A larva is categorized as having SLC bias if it responded with an SLC 3 or 4 times
140 out of the 4 tests. At the highest stimulus intensity that we tested (43 dB), the majority of
141 control larvae (300/448) responded with an SLC within 7 ± 3 ms. There were 43 larvae that
142 showed no bias towards SLC or LLC (2 times SLC and 2 times LLC, bias = 0). There also
143 were larvae that did not perform an SLC ($n = 105$) but did exhibit an LLC, with a mean
144 latency of 54 ± 29 ms (**Figure 2C**). In contrast, all NDL PCB-treated larvae retained a

145 response bias towards LLC at all stimulus intensities tested, which was significantly different
146 from the control ($p < .01$ for the three highest stimulus intensities). However, as we
147 decreased the PCB153 dose, there was an increased shift towards an SLC, yet even at 10
148 nM PCB153 the bias toward LLC was significantly different from the control ($p <.01$ for all
149 stimulus intensities). PCB153 exposures starting at 24 hpf, after many structures of the brain
150 and the neural tube have developed (Smith and Kimelman 2019), had the same effect on
151 startle latency as exposures starting at 4 hpf (**Figure S4B)**.

152 The proportion of control larvae responding to the stimulus (with either an SLC or an LLC)
153 increased from 75.2 ± 33.0% (n = 450) to 95.8 ± 17.0% (n = 457) from the lowest to highest
154 stimulus intensity. In contrast, the proportion of PCB153-, PCB138-, and PCB52-treated
155 larvae that responded remained below 70% at all intensities and were significantly different
156 ($p < .01$) from the control, except for the larvae exposed to 10 nM PCB153 (**Figure 2D**,
157 **Figure S5A**). In contrast to larvae exposed to the NDL PCBs, the larvae exposed to the DL
158 PCB126 and NDL PCB118 had a response latency and rate similar to the control larvae.

159 The kinematics of the C-bend angle differ for the SLC and LLC startle responses, with SLCs
160 exhibiting larger bend angles and faster angular velocities than LLCs (Burgess and Granato
161 2007). We examined the bend angles separately in SLC and LLC occurring after exposure to
162 each PCB. Generally, there were increased bend angles associated with SLC response after
163 NDL PCB exposure, even when there were very few SLC responders. Similarly, there were
164 generally decreased bend angles in the LLC responders after NDL PCB exposures (**Figure**
165 **S6**).

166 **Cellular structures**

167 The proper execution of the startle response relies on hair cells that sense the auditory
168 stimulus, M-cells to integrate the signals, and motor neurons and musculature to execute the
169 startle behavior. Morphological analysis showed that M-cells, motor neurons, and
170 musculature all appeared unaffected by PCB153, but the neurons innervating the hair cells

171 appeared to be swollen (**Figure 3**). The L3 neuromast volume of control larvae was on
172 average 569 μm^3 (*SD* = 125), whereas larvae exposed to PCB153 (1000 nM) had
173 significantly larger L3 neuromast volumes 848 μm^3 (*SD* = 185), $t(48.93) = 6.765$, $p < .0001$
174 (**Figure 3B**). However, the number of hair cells in L3 neuromasts (**Figure 3C**) and the
175 intensity of FM1-43 dye internalized by hair cells (**Figure 3D**) remained unchanged in
176 PCB153-treated larvae in comparison to the control.

177 The presence of functional M-cells is necessary for the SLC startle response. Staining with
178 Mab 3A10 confirmed the presence of M-cells in all PCB153-exposed larvae (21/21) (**Figure**
179 **4A**). We tested the functional responsiveness of the M-cells by applying electric field pulses
180 to head-restrained larvae. This electrical stimulation (**Figure 4B**) bypasses the sensory
181 system and directly activates the M-cell (Tabor et al. 2014). There was no difference
182 detected in response time between control and 1000 nM PCB153-exposed larvae (U =
183 907.5, $p = .489$), demonstrating that the signal transmission from the M-cell to the motor
184 neurons is not disrupted in the PCB153-exposed fish (**Figure 4C**). The fraction responding
185 also was similar in both the DMSO-treated (290/299) and the PCB153-treated (209/219)
186 groups (GLM, $p = .427$; **Figure 4D**). However, the angle of the C-bend evoked by the
187 electrical stimulation was larger in PCB153-exposed larvae ($M = 101.4$, $SD = 38.60$) than in
188 the control larvae ($M = 83.12$, $SD = 24.23$). An unpaired t-test with Welch's correction
189 indicated that this difference was statistically significant, $t(74.27) = 2.679$, $p = .0091$ (**Figure**
190 **4E**). This difference could indicate a PCB153-evoked functional alteration of the M-cell axon
191 or the motor neuron.

192 For rapid and effective axonal signal transmission, proper myelination of axons is key. We
193 did not find PCB153 to reduce cells of the oligodendrocyte lineage in the spinal cord of the
194 *Tg(olig2:EGFP)* transgenic line treated with PCB153, ($t(36) = .553$, $p < .584$). We also did
195 not find any differences in myelination itself in the *Tg(mbp:EGFP-CAAX)* transgenic line
196 treated with PCB153 (**Figure S7**).

197 Proper function and activation of the motor neurons are crucial for the completion of the
198 startle circuit, leading to muscle contractions and the characteristic swimming behaviors. The
199 main caudal primary (CaP), middle primary (MiP), and rostral primary (RoP) motor neurons
200 did not show any distinct structural differences between exposed and control larvae (**Figure**
201 **S8**). The fast muscle fibers in the myotome were not differentially striated in the PCB153
202 treatment group (**Figure S9**). No structural difference in the motor neurons or the myotome
203 was apparent in PCB153-exposed larvae, suggesting that the increased bend angle does
204 not originate from any overt structural differences in the motor neurons or muscle fibers.

205 **Neuronal activity**

206 The release of neurotransmitters into the synaptic cleft is a characteristic process in signal
207 transmission. Both serotonergic and dopaminergic neuromodulators can affect startle latency
208 (Jain et al. 2018), and evidence has been found that NDL PCBs alter these neuromodulators
209 in mammals (e.g. Castoldi et al. 2006; Enayah et al. 2018; Wigestrand et al. 2013). We
210 observed that PCB153 (1000 nM) altered the levels of several neurotransmitters in 6 dpf
211 zebrafish larvae (**Figure 5A**). Significantly increased levels of GABA ($t(6) = 9.719$, $p < .001$),
212 choline-chloride ($t(6) = 8.459$, $p < .001$), 3-methoxytyramine hydrochloride ($t(6) = 3.803$, $p =$
213 $.009$), and L-valine ($t(6) = 3.134$, $p = .020$) were measured in PCB-exposed larvae in
214 comparison to control larvae; while L-Glutamine levels were decreased in comparison to
215 control larvae ($t(6) = 5.966$, $p < .001$).

216 To assess the interaction between PCB exposure and changes in neuromodulatory activity,
217 we pharmacologically manipulated the neurotransmitter levels using dopamine, serotonin,
218 and GABA receptor agonists and antagonists. In control larvae, a 30 min exposure to
219 dopamine precursor L-DOPA and D2-receptor agonist Quinpirole, as well as serotonin
220 precursor 5-HTP, shifted the response to LLC, at multiple intensities tested ($p < .01$; **Figure**
221 **5B**). In contrast, the dopamine antagonist haloperidol exposure induced a shift to SLC in
222 controls across all stimulus intensities ($p < .01$; **Figure 5B**). Haloperidol induced the same
223 shift to SLC in PCB153-exposed larvae ($p < .001$), suggesting that the startle circuit is

224 functional but repressed by PCB (**Figure 5B**). The response rate remained unchanged after
225 exposure to neurotransmitter modulators except for 5-HT, which caused an increase in
226 response probability across all stimulus intensities in control larvae ($p < .01$); quinpirole,
227 which caused a decrease in response probability at the two lowest stimulus intensities in
228 control larvae ($p < .01$); and haloperidol, which caused an increase in response probability at
229 41 dB in PCB153-treated larvae ($p < .01$; **Figure S5**). It is noteworthy, that co-exposure to L-
230 DOPA and PCB153 throughout development increased the startle response rate of PCB153-
231 treated larvae significantly ($p < .01$; **Figure S5C**), yet only induced a significant shift towards
232 SLC at 38 dB ($p < .01$; **Figure S4C**).

233 In the fish brain, a distinct population of serotonergic neurons is found in the posterior
234 tuberculum/hypothalamus, forming a prominent horseshoe-like pattern that is one of several
235 brain regions where 5-HT is synthesized (Oikonomou et al. 2019). To assess whether the
236 development of serotonergic cells in the brain of PCB153 larvae was affected, we performed
237 immunohistochemistry using an antibody for 5-HT (**Figure S10**). The intensity of the
238 fluorescent signal in the hypothalamus was not different, comparing PCB153 ($M = 4.70 \times$
239 10^6, $SD = 2.10 \times 10^6$) with the control ($M = 4.38 \times 10^6$, $SD = 8.1 \times 10^5$) group. This suggests
240 that the serotonergic neurons in this region were not affected.

241 During specific behaviors or sensory experiences, only a small percentage of neurons are
242 active. We analyzed the active neuronal cell populations in PCB153-treated and -untreated
243 larvae, focusing on the rostral hindbrain where the M-cells are located, to assess whether
244 there were changes in neural activity. We examined neuronal activity using the CaMPARI
245 zebrafish line, which contains a protein that upon UV illumination permanently photoconverts
246 from green to red fluorescence in cells with high calcium levels (Fosque et al. 2015). This
247 genomic tool enabled us to look for active neuronal cell populations in larvae during normal
248 swimming movement and in larvae experiencing a vibroacoustic-stimulated startle response.
249 At room temperature (24 °C) no difference in the red to green ratio (F_{red}/F_{green}) was measured
250 comparing control and PCB153-treated larvae, neither when swimming nor startling (**Figure**

251 **S11**). However, when stimulating high neuronal activity by placing the larvae in cold (4 °C)
252 medium, swimming control larvae exhibited a significantly higher F_{red}/F_{green} ratio (*M* = 2.30,
253 *SD* = 0.51) in comparison to swimming PCB153-treated larvae (*M* = 1.70, *SD* = 0.31) on
254 average across two trials (**Figure 5C**). Importantly, the difference between control and
255 PCB153-treated larvae swimming in cold medium was significant in both trials (trial 1: $F(1,$
256 $18) = 121$, *adj. p* = .028 and trial 2 $F(1, 32) = 65.2$, *adj. p* < .001). Similar differences in
257 neuronal activity between control and PCB153 treated larvae were measured for startling
258 larvae (**Figure S11**).

259 Discussion

260 While its use has mostly ended decades ago, PCBs remain a globally important and
261 persistent group of pollutants that continues to impact both wildlife and humans. Prenatal
262 exposure to PCBs is now recognized to contribute to neurobehavioral disorders in humans
263 and potentially other organisms, yet the mechanisms that underlie its neurotoxicity remain
264 largely unknown (Klocke and Lein 2020). Using developmental exposure of zebrafish to
265 PCB153, we identify here an imbalance in dopamine metabolites and GABA mediating
266 mechanosensory deficits in fish, encompassing hearing and touch. The behavioral effect
267 was found to be specific to NDL PCBs and at concentrations relevant for both humans and
268 aquatic life. These findings highlight a so far unrecognized impact of commonly observed
269 concentrations of NDL PCBs on the escape response in fish and link a conserved neurotoxic
270 mechanism to behavioral deficits.

271 We observed a delayed startle response for all NDL PCBs tested and subsequently
272 examined a number of morphological features of the underlying startle circuit anatomy (hair
273 cell, afferent neurons, M-cell, oligodendrocyte lineage cells, myelination, motor neuron,
274 muscle; **Figure 1**), as potentially affected by the NDL PCB153. Only the volume of the
275 neurons that innervate the hair cells showed a measurable deviation from the control
276 condition in PCB153-exposed larvae (**Figure 3**). We thus infer that the enlargement of axon

277 termini is contributing to the neurotoxic potential of NDL PCBs. This is an understudied
278 target of PCB toxicity with only a few studies associating NDL PCB exposure with altered
279 dendritic arborization (Klocke and Lein 2020; Lein et al. 2007; Yang et al. 2009). The direct
280 links to neurobehavioral changes remain to be shown. However, swelling of afferent
281 terminals is associated with hearing deficits in both mammalian models (Puel et al. 1991)
282 and zebrafish (Sebe et al. 2017). Axonal swelling is also a pathology appearing in many
283 neurodegenerative diseases (Coleman 2005), thus exposure to NDL PCBs may be a
284 contributing factor in such diseases.

285 The proper function of the M-cell is essential in transmitting the signal that leads to the rapid
286 startle response. At the structural level, laser-ablation of the M-cell abolishes SLC responses
287 without affecting LLC responses (Lacoste et al. 2015). Our finding that NDL PCB-exposed
288 larvae predominantly exhibit LLC without loss of M-cells (**Figure 2C, 4A**), suggests that the
289 M-cells are receiving a delayed input, are not firing properly, or that the signal propagation
290 downstream of the M-cell is disrupted. To distinguish these, we directly activated the M-cells
291 by applying electrical stimulation to larvae with their heads restrained and found that, unlike
292 auditory stimulation, PCB153-exposed fish had latencies indistinguishable from the controls
293 (**Figure 4C**). Furthermore, direct stimulation of PCB153-exposed larvae resulted in a normal
294 response rate (**Figure 4D**), although the bend angle was significantly increased (**Figure 4E**).
295 These results indicate a proper function of M-cells in NDL PCB-treated larvae. However, the
296 changes in bend angles we observed during these responses could indicate alterations
297 downstream of the M-cells.

298 There is little known about the mechanisms leading to an aberrant turning angle. Since we
299 found no obvious structural impairment downstream of the M-cell (oligodendrocyte lineage
300 cells, myelination, motor neuron, musculature), we speculate that the increased bend angle
301 in electrically stimulated larvae exposed to PCB153 may be linked to a sub-cellular
302 disruption such as gap junctions. It is known that PCBs can alter gap junction function in
303 cells of many organs (Bager et al. 1997; Kang et al. 1996; Machala et al. 2003) including

304 NDL PCB specific inhibition of gap junctional intercellular communication in neural crest cells
305 (Nyffeler et al. 2018) and neuronal stem cells (Kang et al. 2001). Gap junctions are
306 intercellular channels formed by connexins (Cx). RNA sequencing of zebrafish larvae
307 exposed to PCB153 in a similar exposure regime (4-120 hpf) and concentration (10 μM)
308 significantly altered the expression of connexin genes cx28.9, cx42, and cx35b (Aluru et al.
309 2020). Cx35 is expressed on the Mauthner neuron lateral dendrites in zebrafish (Jain et al.
310 2018) and plays a crucial role in regulating spinal motor activity during fast motor behavior of
311 adult mosquitofish (Serrano-Velez et al. 2014). We thus propose that gap junction function
312 could be disrupted, which may be a future study direction using single-cell RNA sequencing
313 or genetically encoded optogenetics that has yet to be developed in a model organism (Dong
314 et al. 2018).

315 Neurotransmitters also play a key role in the startle response. A previous screening of more
316 than 1000 pharmacologically active compounds identified serotonergic and dopaminergic
317 modulators among the largest class of drugs that shift bias between SLC and LLC startle
318 behavior (Jain et al. 2018). Specifically, acute exposure to the D3R agonist (7OHD) shifts the
319 startle bias from LLC to SLC, while exposure to a D3R antagonist (or a 5-HT1AR agonist)
320 shifts bias toward LLC behavior (Jain et al. 2018). Our results extend these findings, showing
321 that 30 minutes of exposure to L-DOPA or 5-HTP induced a shift from SLC to LLC at higher
322 stimulus intensities, as opposed to the D2R antagonist haloperidol, which evoked a shift to a
323 stronger SLC bias at all stimulus intensities (**Figure 5B**). NDL PCBs are thought to affect
324 dopaminergic pathways (Mariussen and Fonnum 2001; Tanaka et al. 2018; Wigestrand et al.
325 2013), which is partly supported by our measurements of catecholamines and traces
326 amines. Specifically, we found that the extracellular dopamine metabolite 3-methoxytyramine
327 hydrochloride and the inhibitory transmitter GABA were significantly increased (**Figure 5A**).
328 The interplay between dopamine and GABA receptor activity is complex. In the mammalian
329 system, dopamine is a direct-acting modulator of $GABA_A$Rs (Hoerbelt et al. 2015). The
330 simultaneous increase of a dopamine metabolite and GABA in PCB153-exposed zebrafish

331 larvae may indicate that increased levels of GABA are a downstream effect of dysregulated
332 dopamine activity. With both dopamine and GABA playing critical roles in motor activity, we
333 hypothesize that PCB153 impairs dopaminergic neurotransmission and subsequently
334 increases GABA levels, leading to the predominant LLC response.

335 Furthermore, we propose that GABA is involved in the swelling of the afferent terminals
336 (**Figure 3**) as GABA activates Cl^- channels leading to an influx of Cl^- accompanied by H_2O
337 (Cesetti et al. 2012; Rungta et al. 2015). The authors report that the osmotic neuronal
338 swelling alters neuronal activity. This study thus provides new evidence that GABA is
339 involved in the neurobehavioral mode of action of higher chlorinated NDL PCBs, as has
340 been shown for lower chlorinated congeners (Fernandes et al. 2010).

341 An important finding of this study is that PCB153-exposed larvae can execute SLC when
342 treated with haloperidol, a D2-antagonist that can increase dopamine turnover in acute
343 exposure (Magnusson et al. 1987), suggesting dopamine turnover as the major disrupted
344 mechanism causing the sensory deficit. There is a large body of evidence showing that NDL
345 PCBs, including PCB153, modulate dopaminergic neurotransmission by inhibiting the
346 dopamine precursor enzyme tyrosine hydroxylase and dopamine synthesis itself, in both
347 neural crest cells and adult laboratory animal models including non-human primates (Dervola
348 et al. 2015; Enayah et al. 2018; Fonnum and Mariussen 2009; Seegal et al. 1990). In
349 zebrafish larvae, PCB153 exposure during development elicited differential expression of
350 nine genes related to the dopamine pathway, including tyrosine hydroxylase 2 (th2) (Aluru et
351 al. 2020). Yet linking such effects to behavior is rare. Tanaka et al. (2018) suggested that the
352 NDL PCB dominant mixture Aroclor 1254 and BDE-47 functionally inhibited dopaminergic
353 neurons in early zebrafish embryos, as increased activity in 26 hpf embryos was inhibited by
354 supplementation with L-tyrosine and L-DOPA (Tanaka et al. 2018).

355 The restoration of the delayed startle phenotype by haloperidol, together with the increased
356 levels of a dopamine metabolite and GABA in PCB153-exposed larvae (**Figure 5A**),
357 indicates that disruption of dopaminergic and GABAergic signaling between neurons of the

358 auditory circuit is the dominant effect of PCB153-mediated aberrant motor behavior. These
359 signaling processes are widely conserved across vertebrate species and are important in
360 human neurological diseases. For example, a recent study found that multiple gene
361 mutations causing defective startle response in zebrafish were also associated with
362 disorders of the locomotor system in humans (Meserve et al. 2020).

363 The localization of the PCB-induced disruption of dopaminergic signal transmission is likely
364 downstream of the hair cells, potentially in the hindbrain. Although dopaminergic neurons
365 innervate lateral line neuromasts, where D1R antagonist reduces the hair cell activity (Toro
366 et al. 2015), we found no difference in the hair cell activity of PCB153-exposed larvae
367 (**Figure 3D**). This is in contrast to the hindbrain, where neuronal activity was reduced in
368 PCB153 exposed CaMPARI zebrafish larvae (**Figure 5C**), indicating a reduced capacity for
369 release or turnover of calcium. Intracellular Ca^{2+} signaling in neurons controls
370 neurotransmitter secretion among many other cellular processes and thus may be indirectly
371 involved in dopamine or GABA regulation. Some NDL PCBs (PCB 95, 138) are known to
372 inhibit voltage-gated calcium channels (Langeveld et al. 2012) contributing to interference
373 with calcium homeostasis and consequently neurotransmission and synaptic plasticity
374 (Brunelli et al. 2012; Campagna et al. 2011; Gafni et al. 2003; Ta et al. 2006).

375 The startle response in fish and amphibians is a fundamental mechanism involved in
376 predator escape. PCB153-exposed zebrafish larvae predominantly responded with an LLC,
377 which not only delays the response, increasing the chance to be caught by a predator but
378 also usually does not displace the animal from its original location (**Figure 2A** and Jain et al.,
379 2018). While survival of predator attack is likely context-dependent and species-specific,
380 quick escape responses increase chances of survival (McCormick et al. 2018), suggesting
381 the highly abundant di-*ortho*-NDL PCBs may provide a substantial selection pressure and
382 thereby could drive evolutionary adaptation. We have observed a significant shift to LLC at
383 concentrations of PCB153 as low as 10 nM (3.6 μg L^{-1}). PCBs are associated with
384 sediments, where concentrations of PCB153 frequently reach multiple μg kg^{-1} (Lai et al.

385 2015). PCB concentrations in organisms may be even higher due to extensive
386 bioconcentration; killifish from New Bedford Harbor have 6.5 to 7 µg of PCB153 per g wet
387 weight (Gräns et al. 2015). All the *ortho*-NDL PCBs tested in this study increased the startle
388 latency. Thus, in the environment, where PCBs occur in mixtures of numerous congeners
389 that likely have additive effects, the combined effect could occur at concentrations lower than
390 that of any single congener. Taken together, these results highlight the importance of the
391 neurotoxic potential of NDL PCBs in the natural environment.

392 Based on the comprehensive approach presented in this study, it can be inferred that
393 PCB153 may alter dopamine signaling, leading to an increase in GABA that ultimately
394 results in swelling of axonal terminals in the auditory circuit. The dysregulation of
395 neurotransmitters is likely the dominating mechanism for the behavioral deficit, as the
396 treatment with the dopamine antagonist haloperidol restored the startle capability of
397 PCB153-treated fish. While the involvement of connexins remains speculative, our findings
398 provide a foothold into the dopamine dysregulating potential of PCB153 and likely other NDL
399 PCBs in sensory-motor processing in developing vertebrates, and link that to motor
400 behavior. In a direct comparison, the present study suggests that the adverse behavioral
401 effects observed are induced by all NDL PCBs tested, but not by the classical DL PCB126.
402 Whether this is true for compounds that are structurally similar to NDL PCBs, such as some
403 PBDEs, is not known and will require further research. A key finding is that the effect of NDL
404 PCBs on the startle latency occurs at concentrations relevant for both environmental and
405 human exposures, thereby exposing a mechanism that is relevant to both a behavior with
406 inherent selection pressures in fish and neurotoxicological diseases in humans. This study
407 therewith provides valuable clues for tackling health effects in humans and wildlife caused by
408 environmental exposure to widespread PCBs.

409 # Materials and Methods

410 **Animal model rationale**

411 Zebrafish have relatively simple neural circuits, particularly for the auditory system. Many of
412 the components of the auditory circuit are homologous in mammals and fish, including hair
413 cells, neural transmission, and lower motorneurons, while the mechanosensory lateral line
414 system and Mauthner (M) cells are exclusively found in fish and a cochlea is only found in
415 mammals. In fish, vibro-acoustic stimuli are first sensed by the hair cell bundles in the
416 auditory, vestibular, and lateral-line systems and are rapidly encoded into trains of action
417 potentials in the afferent neurons (**Figure 1**) (Hudspeth 1985). The signal detected through
418 the sensory hair cells of the lateral line is transmitted through the anterior and posterior
419 lateral line ganglia whereas the auditory input is transmitted through the VIIIth statoacoustic
420 nerve, all of which synapse to the lateral dendrite of the M-cell and two segmental homologs
421 (Nakayama 2004; Pujol-Martí and López-Schier 2013). The signal is propagated down the
422 M-cell axon in the spinal cord to activate the motoneurons leading to a unilateral contraction
423 of the trunk musculature.

424 **Zebrafish lines and husbandry**

425 Zebrafish (*Danio rerio*) were maintained at 28.5 °C and on a 12:12 h light-dark cycle
426 according to the guidelines of the Zebrafish Model Organism Database (ZFIN, http://zfin.org)
427 and institutional guidelines at WHOI and the experimental procedures approved by the
428 Institutional Animal Care and Use Committee (ID Number BI21981.01). Adult zebrafish were
429 fed brine shrimp and Gemma Micro 300 pellets (Skretting) every day. In this study, we used
430 wild-type zebrafish of the AB strain obtained from Zebrafish International Resource Center
431 (ZIRC), as well as several transgenic lines: the photoconvertible calcium indicator line
432 *Tg[elavl3:CaMPARI(W391F+V398L)]*^{jf9} kindly provided by Jessica Plavicki (Brown University,
433 USA), and the transgenic lines *Tg(cntn1b:EGFP-CAAX)* (Panlilio et al. 2021) labeling axons,
434 *Tg(olig2:EGFP)*^{vu12} (Park et al. 2007; Shin et al. 2003) marking oligodendrocyte precursor
435 cell bodies, *Tg(sox10:mRFP)* (Takada et al. 2010) marking oligodendrocyte lineage cells, as

436 well as *Tg(mbp:EGFP-CAAX)* (Almeida et al. 2011) *and Tg(mbp:EGFP)* (gift from Dr. Kelly
437 Monk, generated by Dr. Charles Kaufman in the laboratory of Dr. Leonard Zon, Harvard
438 Medical School, Boston, MA) marking myelin sheaths. Zebrafish eggs were obtained by
439 pairwise breeding and kept in 0.3x Danieau's (17 mM NaCl, 0.2 mM KCl, 0.12 mM $MgSO_4$,
440 0.18 mM $Ca(NO_3)_2$ and 1.5 mM HEPES, pH 7.6) in glass vials at a density of 10 individuals
441 per 10 mL, at a constant water temperature of 28 ± 1˚C and standard 14-h light/10-h dark
442 cycle. The medium was supplemented with 1-Phenyl-2-thiourea (PTU, 0.003% w/v) from 24
443 hours post-fertilization (hpf) onwards to prevent pigment formation when necessary for
444 imaging.

445 **Early-life stage exposure**

446 Fertilized eggs were used for exposures starting at 4 hpf to solvent control (0.1% DMSO,
447 v/v), 2,2′,4,4′,5,5′-hexachlorobiphenyl (PCB153), 2,2′,5,5′-PCB, 2,2′,5,5′-tetrachlorobiphenyl
448 (PCB52), 2,3',4,4',5-pentachlorobiphenyl (PCB118), 2,2’,3,4,4’,5’-hexachlorobiphenyl
449 (PCB138), or 3,3’,4,4’,5-hexachlorobiphenyl (PCB126). Additionally, one exposure with
450 PCB153 was started at 24 hpf, to assess whether effects are induced during or after initial
451 neuronal cell differentiation; sensory neurons send their projection along the ectoderm as
452 early as 16 hpf (Kimmel 1993). The lowest exposure concentration for PCB153 was 10 nM
453 (3.6 ng mL^{-1}), estimated to result in ~5 ng g^{-1} (5 ppm) per zebrafish larva, based on
454 comparison to PCB95 uptake levels (Ranasinghe et al. 2019). PCB153 concentrations found
455 in one study of maternal cord blood serum were 0.27 ng mL^{-1} or 110 ng g^{-1} lipid (Lancz et al.
456 2015b) while other reported concentrations range from 3.7 to 200 ng g^{-1} lipid (Bergonzi et al.
457 2009; Herbstman et al. 2007; Lancz et al. 2015b; Patel et al. 2018). We also used higher
458 exposure concentrations of PCB153 including 30 nM, 100 nM, and 1000 nM, which are
459 found in fish of contaminated ecosystems such as the New Bedford Harbor in
460 Massachusetts, USA (Gräns et al. 2015). For PCB52, PCB118, and PCB138, a
461 concentration of 1000 nM was chosen, to compare to the highest effect concentration of
462 PCB153. The DL-PCB126 is cardioteratogenic in the low nanomolar range. To avoid

463 malformations, a concentration of 1 nM was chosen, which is still highly effective at
464 activating the aryl hydrocarbon receptor and the expression of AHR target genes. Exposures
465 were refreshed daily until four days post-fertilization (dpf) and all larvae were kept in
466 Danieau's from 5 to 6 dpf. All imaging and behavioral assays were performed at 6 dpf,
467 except for the touch assay, which was performed at 26 hpf. For all behavioral assays, only
468 larvae with an inflated swim bladder were used.

469 The influence of neurotransmitters on the startle behavior was assessed by exposures to
470 compounds known to interfere with monoamines. At 6 dpf, larvae were evaluated for their
471 startle behavior and then immersed in the dopamine precursors L-DOPA (1 mM) or L-
472 tyrosine (1 mM), dopamine receptor agonist quinpirole (10 µM), dopamine D2-receptor
473 antagonist and GABA receptor modulator haloperidol (10 µM), endogenous serotonin 5-HT
474 (10 µM), and serotonin precursor 5-HTP (1 mM) for 30 min in the well plate before assessing
475 the startle behavior again. Additionally, the effect of neurotransmitter modulation during
476 development on startle response was assessed by exposing larvae from 3 to 120 hpf to L-
477 DOPA (1 mM), L-tyrosine (1 mM), and quinpirole (10 µM).

478 **Behavioral assays**

479 Larval locomotion was monitored using the Noldus Daniovison system (Noldus Information
480 Technology, Leesburg, VA, USA) using 6-dpf larvae distributed in 48-well plates (1 larva per
481 well). After an acclimation period of 40 minutes in the illuminated chamber, spontaneous
482 swimming activity was tracked for 10 minutes. Following the spontaneous swimming, three
483 alternating cycles of dark and light conditions (10 minutes each) were run. The experiment
484 was repeated three times with cohorts from separate breeding events (n = 24 per group and
485 breeding event). Video data were recorded with 30 frames per second via an infrared
486 camera. Obtained data were analyzed with the supplied software EthoVision XT® 12
487 (Noldus. Inc.).

488 The activity of Rohon-Beard sensory neurons was tested at 26 hpf by lightly touching
489 DMSO- and 1000 nM PCB153-exposed embryos (*n* = 10 per group and breeding event)
490 using a piece of fishing line affixed to a glass pipette. Each embryo was touched ten times
491 and the response was scored as follows: 0, no response; 0.5, light tail flicking response, 1,
492 coiling in the opposite direction of the touch stimulus, yielding a score of a maximum of 10
493 per embryo. The experiment was repeated twice with cohorts from separate breeding
494 events.

495 Vibro-acoustic startle response was assessed as described previously (Panlilio et al. 2021).
496 Briefly, the acoustic stimuli were delivered by a vibrational exciter producing acoustic
497 vibrations at a frequency of 1000 Hz for a duration of 2 ms at four different amplitudes (32,
498 38, 41, 43 dB). For each amplitude, the stimulus was delivered four times, spaced 20
499 seconds apart, to a 4 x 4 well-plate mounted on top of the speaker, each well containing an
500 individual larva. The response was tracked with a high-speed camera (Edgertronic SC1) at
501 1000 frames s^{-1} for 250 ms (13 ms before and 237 ms after the stimulus). PulsePal was used
502 to synchronize the camera recording to the acoustic stimuli using a TTL pulse. Automated
503 analysis of larval movement kinematics (response frequency, latency, turning angle) was
504 performed using the FLOTE software package (Burgess and Granato 2007). Each treatment
505 group was assessed at least three times with eggs from different clutches. The total replicate
506 numbers are stated in **Table S1 (Supplemental Material)**.

507 A startle response in fish can be executed with a short latency C-bend (SLC) or long latency
508 C-bend (LLC), with the SLC being the more frequent response at higher stimulus intensities.
509 The cut-off time between SLC and LLC can vary depending on environmental conditions
510 such as temperature and has been determined empirically for this experiment using a
511 Gaussian mixture model (Panlilio et al. 2020; **Figure S12**). Responses within 15 ms were
512 categorized as SLC, latencies greater than 15 ms as LLC. Following this classification, the
513 median response type (Relative Startle Bias) for each responsive fish was determined for
514 each stimulus intensity (32, 38, 41, and 43 dB). Bias per individual fish was calculated as

515 (frequency of SLC – frequency of LLC) / total responses. Pure SLC responses result in a
516 value of +1, while pure LLC responses are a value of -1 (Jain et al. 2018).

517 Electric field pulses (EFPs) directly activate the M-cells (Tabor et al. 2014). M-cell
518 functionality was assessed by using head-restrained larvae (*n* = 46 per treatment group). For
519 each run, one control and one PCB-exposed larva had their heads embedded in 1.5%
520 agarose, side-by-side, with their tails free to move. Seven consecutive EFPs (4.4 V cm^{-1} for 2
521 ms, square pulse) were applied with a recovery time of 20 s in between pulses. Response
522 frequency, latency, and bend angle were tracked using FLOTE.

523 **Larval growth**

524 Larval length (from snout to the tail-fin end) was measured in DMSO (*n* = 57) and 1000 nM
525 PCB153 (*n* = 51) exposed larvae using ImageJ. The experiment was performed three times
526 with embryos from different clutches.

527 **FM1-43 labeling of functional hair cells**

528 The vital fluorescent dye FM1-43 (n-(3-triethylammoniumpropyl)-4-(4-(dibutylamino)-styryl)
529 pyridinium dibromide; Invitrogen) specifically labels hair cells in the lateral line and inner ear
530 of vertebrates by entering through open mechanotransduction channels and filling the
531 cytoplasm of hair cells (Meyers et al. 2003). At 6 dpf, zebrafish larvae of 1000 nM PCB153-
532 exposed (*n* = 32) and unexposed (*n* = 28) groups were immersed in Danieau's
533 supplemented with 3 μM FM1-43 for 30 s, rinsed three times in Danieau's, anesthetized in 1
534 mM 3-amino-benzoic acid (Tricaine), and mounted in 1.5% low melting agarose for confocal
535 imaging of the L3 neuromast. The experiment was performed three times independently.

536 **Visualization of M-cells, kinocilia, and muscle fibers, neurons, oligodendrocyte lineage**
537 **cells, and neuronal activity**

538 Whole-mount immunohistochemistry of zebrafish larvae and brains was performed following
539 standard procedures. Briefly, 10 AB larvae per exposure group were treated as described
540 above and subsequently fixed in 4% paraformaldehyde (PFA) in PBS overnight at 4 ˚C. For

541 labeling brain tissue, larval brains were dissected before continuing with the protocol.
542 Multiple rinsing steps in PBS containing either 0.5% Triton-X100 or 0.1% Tween-20 (PBST)
543 for larvae or brains, respectively, was followed by an antigen retrieval step in 150 mM Tris
544 HCl (pH 9.0) at 70 °C (Inoue and Wittbrodt 2011), and a permeabilization step using
545 proteinase K (10 µg/mL for 3 minutes). Subsequently, the samples were blocked in blocking
546 solution (10% Normal Goat Serum, 1% DMSO, 1% BSA, 88% PBST) for 1 h and then
547 stained with blocking solution supplemented with the primary antibody for three days at 4 ˚C.
548 The primary anti-neurofilament mouse monoclonal antibody 3A10 (Developmental
549 Hybridoma Bank; 1:100 dilution) was used to label a subset of hindbrain spinal cord
550 projecting neurons such as the M-cell neurons (DMSO *n* = 23, PCB153 *n* = 21). The anti-
551 5HT rabbit polyclonal antibody (Sigma-Aldrich, #S5545, 1:500) was used to label
552 serotonergic cells (DMSO *n* = 16, PCB153 *n* = 13). The anti-acetylated alpha-tubulin mouse
553 polyclonal antibody (Sigma-Aldrich, #T6793, 1:1000 dilution) was used to label kinocilia and
554 hair cell innervating neurons (DMSO *n* = 25, PCB153 *n* = 24). After several washing steps, in
555 PBST, the samples were incubated with Alexa Fluor 488- or 594-conjugated goat-anti-
556 mouse or goat-anti-rabbit secondary antibodies (Abcam, 1:500 dilution) overnight at 4 ˚C and
557 rinsed several times in PBST before mounting in ProLong Diamond Antifade mountant
558 (Invitrogen) for imaging. For visualization of skeletal muscle fibers (DMSO *n* = 20, PCB153 *n*
559 = 20), larvae were fixed as above, followed by permeabilization in 5% Triton-X for overnight
560 and incubation in phalloidin Alexa-546 conjugate (Invitrogen, 1:500). All staining experiments
561 were repeated three times with larvae from independent clutches.

562 The *Tg(cntn1b:EGFP-CAAX)* transgenic line was used to image the cell bodies of neurons
563 that innervate the hair cells at the L3 position in the lateral line (DMSO *n* = 22, PCB153 *n* =
564 20, two independent experiments). The axons of the main caudal primary motoneurons were
565 visualized using the *Tg(olig2:EGFP)* transgenic line (DMSO: *n* = 21, PCB153: *n* = 18). The
566 double transgenic *Tg(olig2:EGFP) x Tg(sox10:mRFP)* was used to quantify oligodendrocyte
567 lineage cells in the spinal cord of in DMSO (*n* = 22) and 1000 nM PCB153 (*n* = 16) treated

568 larvae (Shin et al. 2003). All larvae were anesthetized in tricaine (0.16% MS222) before
569 mounting laterally in 1.5% low melting agarose on a glass-bottom microscopy dish (MatTek).
570 Fluorescently labeled cell bodies were imaged at the distal end of the intestine, around the
571 L3 neuromast. All experiments were performed three times independently.

572 Neuronal activity in DMSO- and PCB153-treated larvae was visualized using the CaMPARI
573 (*elavl3*:CaMPARI) transgenic zebrafish line with an engineered fluorescent protein that
574 permanently photoconverts from green to red in the presence of elevated calcium and UV
575 light (Fosque et al. 2015). Photoconversion was achieved by mounting an LED light (405 nm;
576 LEDSupply) between the speaker and a custom-made 3-well plate containing the freely
577 swimming larvae (DMSO- and PCB153-treated). Larvae of the same treatment were divided
578 into two batches: one was photoconverted in medium at room temperature (RT) and the
579 other one at 4˚C to elicit high neuronal activity. Photoconversion was achieved by shining the
580 LED light for 10 sec either with one vibrational stimulus of 43 dB at the start or without
581 stimulus. Subsequently, larvae were anesthetized, embedded in agarose, and whole brains
582 imaged using the 10x objective. The experiment was performed twice (*n* = 11-16 per
583 treatment group).

584 **Image acquisition and processing**

585 Whole-brain, hair cells, M-cell, and motor neurons were imaged on a Zeiss LSM 800
586 confocal system with a 10x/0.45 Plan-Apochromat, 20x/0.8 Plan-Apochromat, or 63x/1.2 C-
587 Apochromat water immersion objective. Airy scan was applied for hair cell imaging at 63x. Z-
588 stacks were merged to a single plane by maximal intensity projection using Fiji (Schindelin et
589 al. 2012).

590 The number of *olig2* cells dorsal of the spinal cord (DMSO *n* = 22, 1000 nM PCB153 *n* = 16)
591 was counted in confocal image stacks using the 3D projection of the Zeiss Zen blue
592 software. Myelination was evaluated after imaging the spinal cord (DMSO *n* = 26, 1000 nM
593 PCB153 *n* = 27) using the 20x objective and scored for deficits according to Panlilio et al.

594 2020. Representative myelination was imaged at 40x. The intensity of serotonergic neurons
595 in the brain (DMSO *n* = 16, 1000 nM PCB153 *n* = 13) was measured performing a Sum
596 Slices Z-projection followed by drawing a ROI around the 5-HT immuno-responsive cells,
597 and per image, three random squares (area size = 10.65 x 10.65) within the non-fluorescent
598 area of the ROI for background subtraction (for orientation see **Figure S12**). Similarly, the
599 FM1-43 intensity was measured drawing a ROI around the fluorescent hair cells and
600 measuring the background in three random squares (DMSO *n* = 20, 1000 nM PCB153 *n* =
601 20). Corrected total cell fluorescence (CTCF) was calculated according to the formula:
602 Integrated density - (ROI x Mean fluorescence of background readings). For quantification of
603 active neurons in the brain of freely swimming and startling CaMPARI zebrafish larvae, Sum
604 Slices Z-projection were analyzed for red fluorescence intensity in the rostral hindbrain (for
605 orientation see **Figure S13**). To calculate the volume of hair cell innervating neurons,
606 automatic image thresholding with fixed minimum and maximum threshold values (30; 255)
607 using the Otsu method) was applied to all images. Subsequently, image stacks were
608 analyzed using an imageJ macro looping through the stack and summing the area
609 measurements, then multiplying this sum by the depth of each slice (DMSO *n* = 30, 1000 nM
610 PCB153 *n* = 29). The presence of primary motor neurons was confirmed using the Simple
611 Neurite Tracer plugin in Fiji (DMSO *n* = 21, 1000 nM PCB153 *n* = 18). All image evaluations
612 and quantifications were done without the knowledge of the experimental condition of the
613 specimens.

614 **Neurotransmitter analysis**

615 The analysis of neurotransmitters, including histamine, L-histidine, L-glutamic acid, gamma-
616 aminobutyric acid (GABA), acetylcholine, L-DOPA, 3-methoxytyramine, serotonin, 5-
617 hydroxyindole-3-acetic acid, glycine, L-glutamine, L-valine, 3-hydroxytyramine and choline,
618 was performed with a method developed in a previous study (Zhao et al. 2020). Briefly, the
619 zebrafish embryo samples were spiked with 100 ppb isotope-labeled internal standards and
620 then homogenized. The homogenized tissue samples were extracted with 200 µL of 80:20

621 v/v ACN/Milli-Q water containing 0.1% formic acid and 1% ascorbic acid and 200 μL ACN.
622 After protein precipitation, the supernatants were dried and redissolved in 100 μL of Milli-Q
623 water containing 0.1% formic acid for UHPLC-MS/MS analysis. Neurotransmitters were
624 quantified by a high-performance liquid chromatography system coupled to a Q-Exactive
625 plus quadrupole-Orbitrap mass spectrometer (UHPLC-Q-Orbitrap, Thermo fisher, US). The
626 separation of neurotransmitters was carried out with an Acquity UPLC HSS T3 column with
627 Milli-Q water containing 0.1% formic acid and ACN containing 0.1% formic acid as mobile
628 phase. The MS acquisition was performed in the full scan mode and parallel reaction
629 monitoring mode. The experiment was performed once (*n* = 4 per treatment group).

630 **Statistical Analyses**

631 All statistical analyses were conducted using Graph Pad Prism 8.4 except some of the startle
632 behavior analysis, which was completed in R. All quantitative data were tested for normality
633 using the Shapiro-Wilk test, and if there were an unequal number of subjects between
634 groups, the data were tested for homogeneity in variances using the Brown-Forsythe test. All
635 treatment groups were compared to respective control groups.

636 Responsiveness to auditory stimuli (response or not) and startle type (SLC vs. LLC) was
637 modeled in R (version 4.0.2) using a binomial generalized linear mixed effect model (glmer()
638 from the lme4 R package) (Bates et al. 2015). The response to electrical stimulus was
639 modeled using glm() from the lme4 R package. For the auditory response, we included
640 treatment as a fixed effect and the replicate experimental trials as a random effect. The
641 model specification for “fraction responding” was as follows: Responders ~ TreatmentGroup
642 + (TreatmentGroup|trial). The model specification for “startle bias” was as follows:
643 SLCorLLCresponse ~ TreatmentGroup + stimdB + (1|trial). The data were analyzed fitting
644 the model for each stimulus intensity independently. The model specification for the electrical
645 stimulation is as follows: Responders ~ TreatmentGroup.

646 To assess treatment differences of normal data with three or more groups (fluorescence
647 intensity CaMPARI), ANOVA comparisons were performed followed by a multiple
648 comparison using the Tukey's correction to adjust the critical values. A Tukey-corrected *p*-
649 value < .05 was considered statistically significant. For normal data with heterogeneity
650 within-group variances (LLC bend angle), a Welch ANOVA followed by a Dunnett's T3
651 multiple comparison test was performed. For non-normal data with three or more groups
652 (SLC bend angle), a Kruskal-Wallis followed by the Dunn's multiple comparison test was
653 performed. For normal data with two groups (length, mean latency, bend angle in e-stim,
654 oligodendrocyte lineage cell count, 5-HT intensity), an unpaired two-tailed t-test with Welch's
655 correction (Welch's t-test) was performed. The nonparametric scoring data of the touch
656 assay and latency in e-stim was analyzed using a two-tailed Mann-Whitney test. The data
657 are presented as mean ± *SD* with single data points (replicates) superimposed on the graph
658 unless specified in the figure legend.

659 **CRediT authorship contribution statement**

660 **Nadja R. Brun:** Conceptualization, Methodology, Formal analysis, Investigation, Writing -
661 original draft, Writing - review & editing, Visualization, Funding acquisition. **Jennifer M.**
662 **Panlilio:** Conceptualization, Methodology, Software, Formal analysis, Investigation, Writing -
663 review & editing, Funding acquisition. **Kun Zhang:** Methodology, Investigation, Writing -
664 review & editing, Funding acquisition. **Yanbin Zhao:** Methodology, Investigation, Writing -
665 review & editing, Funding acquisition. **Evgeny Ivashkin:** Methodology, Investigation. **John J.**
666 **Stegeman:** Conceptualization, Writing - review & editing, Funding acquisition. **Jared V.**
667 **Goldstone:** Conceptualization, Writing - review & editing, Project administration.

668 **Funding**

669 This work was supported by the Swiss National Science Foundation P2EZP2_165200 (NRB),
670 the Boston University Superfund Research Program NIH 5P42ES007381 (JJS and JVG), the

671 Woods Hole Center for Oceans and Human Health (NIH: P01ES021923 and P01ES028938;
672 NSF: OCE-1314642 and OCE-1840381) (NRB, JMP, and JJS), and the National Natural
673 Science Foundation of China 22006099 (KZ and YZ) and the Shanghai Pujiang Program
674 19PJ1404900 (KZ and YZ).

675 Acknowledgments

676 The authors would like to thank Neel Aluru for the helpful discussion and providing the confocal
677 microscope and Ed Levin and Mark Hahn for critically reading the manuscript and making
678 valuable suggestions.

679 References

680 Almeida RG, Czopka T, Ffrench-Constant C, Lyons DA. 2011. Individual axons regulate the
681 myelinating potential of single oligodendrocytes in vivo. Development 138:4443–50;
682 doi:10.1242/dev.071001.

683 Aluru N, Krick KS, Mcdonald AM, Karchner SI. 2020. Developmental exposure to PCB153
684 (2,2′,4,4′,5,5′-hexachlorobiphenyl) alters circadian rhythms and the expression of clock
685 and metabolic genes. Toxicol Sci 173:41–52; doi:10.1093/toxsci/kfz217.

686 Bager Y, Lindebro MC, Martel P, Chaumontet C, Wärngård L. 1997. Altered function,
687 localization and phosphorylation of gap junctions in rat liver epithelial, IAR 20, cells after
688 treatment with PCBs or TCDD. Environ Toxicol Pharmacol 3:257–266;
689 doi:10.1016/S1382-6689(97)00021-5.

690 Bates D, Mächler M, Bolker B, Walker S. 2015. Fitting Linear Mixed-Effects Models using
691 lme4. J Stat Softw 67:1–48; doi:10.18637/jss.v067.i01.

692 Berger DF, Lombardo JP, Jeffers PM, Hunt AE, Bush B, Casey A, et al. 2001. Hyperactivity
693 and impulsiveness in rats fed diets supplemented with either Aroclor 1248 or PCB-
694 contaminated St. Lawrence river fish. Behav Brain Res 126:1–11; doi:10.1016/S0166-
695 4328(01)00244-3.

696 Bergonzi R, Specchia C, Dinolfo M, Tomasi C, De Palma G, Frusca T, et al. 2009.
697 Distribution of persistent organochlorine pollutants in maternal and foetal tissues: Data
698 from an Italian polluted urban area. Chemosphere 76:747–754;
699 doi:10.1016/j.chemosphere.2009.05.026.

700 Boix J, Cauli O, Felipo V. 2010. Developmental exposure to polychlorinated biphenyls 52,
701 138 or 180 affects differentially learning or motor coordination in adult rats. Mechanisms
702 involved. Neuroscience 167:994–1003; doi:10.1016/j.neuroscience.2010.02.068.

703 Boucher O, Muckle G, Bastien CH. 2009. Prenatal exposure to polychlorinated biphenyls: A
704 neuropsychologic analysis. Environ Health Perspect 117:7–16; doi:10.1289/ehp.11294.

705 Brunelli L, LLansola M, Felipo V, Campagna R, Airoldi L, De Paola M, et al. 2012. Insight
706 into the neuroproteomics effects of the food-contaminant non-dioxin like polychlorinated
707 biphenyls. J Proteomics 75:2417–2430; doi:10.1016/J.JPROT.2012.02.023.

708 Burgess HA, Granato M. 2007. Sensorimotor gating in larval zebrafish. J Neurosci 27:4984–
709 4994; doi:10.1523/JNEUROSCI.0615-07.2007.

710 Campagna R, Brunelli L, Airoldi L, Fanelli R, Hakansson H, Heimeier RA, et al. 2011.
711 Cerebellum Proteomics addressing the cognitive deficit of rats perinatally exposed to
712 the food-relevant polychlorinated biphenyl 138. Toxicol Sci 123:170–179;
713 doi:10.1093/toxsci/kfr156.

714 Castoldi AF, Blandini F, Randine G, Samuele A, Manzo L, Coccini T. 2006. Brain
715 monoaminergic neurotransmission parameters in weanling rats after perinatal exposure
716 to methylmercury and 2,2′,4,4′,5,5′-hexachlorobiphenyl (PCB153). Brain Res 1112:91–
717 98; doi:10.1016/j.brainres.2006.07.022.

718 Cesetti T, Ciccolini F, Li Y. 2012. GABA not only a neurotransmitter: Osmotic regulation by
719 GABA AR signaling. Front Cell Neurosci 6; doi:10.3389/fncel.2012.00003.

720 Chen Y-CJ, Guo Y-L, Hsu C-C, Rogan WJ. 1992. Cognitive development of Yu-Cheng ('Oil
721 Disease') children prenatally exposed to heat-degraded PCBs. JAMA J Am Med Assoc
722 268:3213; doi:10.1001/jama.1992.03490220057028.

723 Coccini T, Roda E, Castoldi AF, Poli D, Goldoni M, Vettori MV, et al. 2011. Developmental
724 exposure to methylmercury and 2,2′,4,4′,5,5′-hexachlorobiphenyl (PCB153) affects
725 cerebral dopamine D1-like and D2-like receptors of weanling and pubertal rats. Arch
726 Toxicol 85:1281–1294; doi:10.1007/s00204-011-0660-y.

727 Coleman M. 2005. Axon degeneration mechanisms: Commonality amid diversity. Nat Rev
728 Neurosci 6:889–898; doi:10.1038/nrn1788.

729 Crofton KM, Ding D-L, Padich R, Taylor M, Henderson D. 2000. Hearing loss following
730 exposure during development to polychlorinated biphenyls: A cochlear site of action.
731 Hear Res 144:196–204; doi:10.1016/S0378-5955(00)00062-9.

732 Dervola KSN, Johansen EB, Walaas SI, Fonnum F. 2015. Gender-dependent and genotype-
733 sensitive monoaminergic changes induced by polychlorinated biphenyl 153 in the rat
734 brain. Neurotoxicology 50:38–45; doi:10.1016/J.NEURO.2015.07.004.

735 Dong A, Liu S, Li Y. 2018. Gap junctions in the nervous system: Probing functional
736 connections using new imaging approaches. Front Cell Neurosci 12:1–9;
737 doi:10.3389/fncel.2018.00320.

738 Enayah SH, Vanle BC, Fuortes LJ, Doorn JA, Ludewig G. 2018. PCB95 and PCB153
739 change dopamine levels and turn-over in PC12 cells. Toxicology 394:93–101;
740 doi:10.1016/j.tox.2017.12.003.

741 Ennaceur S, Gandoura N, Driss MR. 2008. Distribution of polychlorinated biphenyls and
742 organochlorine pesticides in human breast milk from various locations in Tunisia: Levels

743 of contamination, influencing factors, and infant risk assessment. Environ Res 108:86–
744 93; doi:10.1016/J.ENVRES.2008.05.005.

745 Fernandes ECA, Hendriks HS, Van Kleef RGDM, Van Den Berg M, Westerink RHS. 2010.
746 Potentiation of the human GABAA receptor as a novel mode of action of lower-
747 chlorinated non-dioxin-like PCBs. Environ Sci Technol 44:2864–2869;
748 doi:10.1021/es902321a.

749 Fonnum F, Mariussen E. 2009. Mechanisms involved in the neurotoxic effects of
750 environmental toxicants such as polychlorinated biphenyls and brominated flame
751 retardants. J Neurochem 111:1327–1347; doi:10.1111/j.1471-4159.2009.06427.x.

752 Fosque BF, Sun Y, Dana H, Yang C, Ohyama T, Tadross MR, et al. 2015. Labeling of active
753 neural circuits in vivo with designed calcium integrators. Science 347: 755–760.

754 Gafni J, Wong PW, Pessah IN. 2003. Non-coplanar 2,2',3,5',6-pentachlorobiphenyl (PCB 95)
755 amplifies ionotropic glutamate receptor signaling in embryonic cerebellar granule
756 neurons by a mechanism involving ryanodine receptors. Toxicol Sci 77:72–82;
757 doi:10.1093/toxsci/kfh004.

758 Goldey ES, Kehn LS, Lau C, Rehnberg GL, Crofton KM. 1995. Developmental exposure to
759 polychlorinated biphenyls (Aroclor 1254) reduces circulating thyroid hormone
760 concentrations and causes hearing deficits in rats. Toxicol Appl Pharmacol 135:77–88;
761 doi:10.1006/TAAP.1995.1210.

762 Grandjean P, Landrigan PJ. 2014. Neurobehavioural effects of developmental toxicity.
763 Lancet Neurol 13:330–338; doi:10.1016/S1474-4422(13)70278-3.

764 Gräns J, Wassmur B, Fernández-Santoscoy M, Zanette J, Woodin BR, Karchner SI, et al.
765 2015. Regulation of pregnane-X-receptor, CYP3A and P-glycoprotein genes in the
766 PCB-resistant killifish (Fundulus heteroclitus) population from New Bedford Harbor.
767 Aquat Toxicol 159:198–207; doi:10.1016/j.aquatox.2014.12.010.

768 Herbstman JB, Sjödin A, Apelberg BJ, Witter FR, Patterson DG, Halden RU, et al. 2007.
769 Determinants of prenatal exposure to polychlorinated biphenyls (PCBs) and
770 polybrominated diphenyl ethers (PBDEs) in an urban population. Environ Health
771 Perspect 115:1794–1800; doi:10.1289/ehp.10333.

772 Hoerbelt P, Lindsley TA, Fleck MW. 2015. Dopamine directly modulates GABAA receptors. J
773 Neurosci 35:3525–3536; doi:10.1523/JNEUROSCI.4390-14.2015.

774 Howe K, Clark MD, Torroja CF, Torrance J, Berthelot C, Muffato M, et al. 2013. The
775 zebrafish reference genome sequence and its relationship to the human genome.
776 Nature 496:498–503; doi:10.1038/nature12111.

777 Hudspeth A. 1985. The cellular basis of hearing: the biophysics of hair cells. Science
778 230:745–752; doi:10.1126/science.7414321.

779 Inoue D, Wittbrodt J. 2011. One for all-a highly efficient and versatile method for fluorescent
780 immunostaining in fish embryos. PLoS One 6:1–7; doi:10.1371/journal.pone.0019713.

781 Jain RA, Wolman MA, Marsden KC, Nelson JC, Shoenhard H, Echeverry FA, et al. 2018. A
782 forward genetic screen in zebrafish identifies the G-protein-coupled receptor CaSR as a

783 modulator of sensorimotor decision making. Curr Biol 28:1357-1369.e5;
784 doi:10.1016/j.cub.2018.03.025.

785 Johansen EB, Fonnum F, Lausund PL, Walaas SI, Bærland NE, Wøien G, et al. 2014.
786 Behavioral changes following PCB 153 exposure in the Spontaneously Hypertensive rat
787 - an animal model of Attention-Deficit/Hyperactivity disorder. Behav Brain Funct 10:1–
788 19; doi:10.1186/1744-9081-10-1.

789 Jusko TA, Sisto R, Iosif A-M, Moleti A, Wimmerová S, Lancz K, et al. 2014. Prenatal and
790 postnatal serum PCB concentrations and cochlear function in children at 45 months of
791 age. Environ Health Perspect 122:1246–1252; doi:10.1289/ehp.1307473.

792 Kang K-S, Park J-E, Ryu D-Y, Lee Y-S. 2001. Effects and neuro-toxic mechanisms of
793 2,2',4,4',5,5'-hexachlorobiphenyl and endosulfan in neuronal stem cells. J Vet Med Sci
794 63:1183–1190; doi:10.1292/jvms.63.1183.

795 Kang KS, Wilson MR, Hayashi T, Chang CC, Trosko JE. 1996. Inhibition of gap junctional
796 intercellular communication in normal human breast epithelial cells after treatment with
797 pesticides, PCBs, and PBBs, alone or in mixtures. Environ Health Perspect 104:192–
798 200; doi:10.1289/ehp.96104192.

799 Keil KP, Sethi S, Lein PJ. 2019. Sex-Dependent Effects of 2,2′,3,5′,6-Pentachlorobiphenyl on
800 Dendritic Arborization of Primary Mouse Neurons. Toxicol Sci 168:95–109;
801 doi:10.1093/toxsci/kfy277.

802 Kimmel CB. 1993. Patterning the brain of the zebrafish embryo. Annu Rev Neurosci 16:707–
803 732; doi:10.1146/annurev.ne.16.030193.003423.

804 Klocke C, Lein PJ. 2020. Evidence implicating non-dioxin-like congeners as the key
805 mediators of polychlorinated biphenyl (PCB) developmental neurotoxicity. Int J Mol Sci
806 21; doi:10.3390/ijms21031013.

807 Lacoste AMB, Schoppik D, Robson DN, Haesemeyer M, Portugues R, Li JM, et al. 2015. A
808 convergent and essential interneuron pathway for mauthner-cell-mediated escapes.
809 Curr Biol 25:1526–1534; doi:10.1016/j.cub.2015.04.025.

810 Lai Z, Li X, Li H, Zhao L, Zeng Y, Wang C, et al. 2015. Residual distribution and risk
811 assessment of polychlorinated biphenyls in surface sediments of the Pearl River Delta,
812 South China. Bull Environ Contam Toxicol 95:37–44; doi:10.1007/s00128-015-1563-z.

813 Lancz K, Hertz-Picciotto I, Jusko TA, Murínová Ľ, Wimmerová S, Šovčíková E, et al. 2015a.
814 Duration of breastfeeding and serum PCB 153 concentrations in children. Environ Res
815 136:35–39; doi:10.1016/j.envres.2014.09.036.

816 Lancz K, Palkovičováa L, Patayová H, Drobná B, Wimmerová S, Šovčíková E, et al. 2015b.
817 Ratio of cord to maternal serum PCB concentrations in relation to their congener-
818 specific physicochemical properties. Int J Hyg Env Heal 218:91–98;
819 doi:doi:10.1016/j.ijheh.2014.08.003.

820 Landrigan PJ, Fuller R, Acosta NJR, Adeyi O, Arnold R, Basu N, et al. 2018. The Lancet
821 Commission on pollution and health. Lancet 391:462–512; doi:10.1016/S0140-
822 6736(17)32345-0.

823 Langeveld WT, Meijer M, Westerink RHS. 2012. Differential effects of 20 non-dioxin-like
824 PCBs on basal and depolarization-evoked intracellular calcium levels in PC12 cells.
825 Toxicol Sci 126:487–496; doi:10.1093/toxsci/kfr346.

826 Lein PJ, Yang D, Bachstetter AD, Tilson HA, Harry GJ, Mervis RF, et al. 2007. Ontogenetic
827 alterations in molecular and structural correlates of dendritic growth after developmental
828 exposure to polychlorinated biphenyls. Environ Health Perspect 115:556–563;
829 doi:10.1289/ehp.9773.

830 Lilienthal H, Heikkinen P, Andersson PL, van der Ven LTM, Viluksela M. 2011. Auditory
831 effects of developmental exposure to purity-controlled polychlorinated biphenyls
832 (PCB52 and PCB180) in rats. Toxicol Sci 122:100–111; doi:10.1093/toxsci/kfr077.

833 Lilienthal H, Korkalainen M, Andersson PL, Viluksela M. 2015. Developmental exposure to
834 purity-controlled polychlorinated biphenyl congeners (PCB74 and PCB95) in rats:
835 Effects on brainstem auditory evoked potentials and catalepsy. Toxicology 327:22–31;
836 doi:10.1016/J.TOX.2014.11.004.

837 Liu YC, Hale ME. 2017. Local spinal cord circuits and bilateral mauthner cell activity function
838 together to drive alternative startle behaviors. Curr Biol 27:697–704;
839 doi:10.1016/j.cub.2017.01.019.

840 Machala M, Bláha L, Vondráček J, Trosko JE, Scott J, Upham BL. 2003. Inhibition of gap
841 junctional intercellular communication by noncoplanar polychlorinated biphenyls:
842 Inhibitory potencies and screening for potential Mode(s) of Action. Toxicol Sci 76:187–
843 195; doi:10.1093/TOXSCI.

844 Magnusson O, Mohringe B, Thorell G, Lake-Bakaar DM. 1987. Effects of the dopamine D2
845 selective receptor antagonist remoxipride on dopamine turnover in the rat brain after
846 acute and repeated administration. Pharmacol Toxicol 60:368–373; doi:10.1111/j.1600-
847 0773.1987.tb01529.x.

848 Mariussen E, Fonnum F. 2001. The effect of polychlorinated biphenyls on the high affinity
849 uptake of the neurotransmitters, dopamine, serotonin, glutamate and GABA, into rat
850 brain synaptosomes. Toxicology 159:11–21; doi:10.1016/S0300-483X(00)00374-7.

851 Maximino C, Herculano AM. 2010. A review of monoaminergic neuropsychopharmacology in
852 zebrafish. Zebrafish 7:359–378; doi:10.1089/zeb.2010.0669.

853 McCormick MI, Fakan E, Allan BJM. 2018. Behavioural measures determine survivorship
854 within the hierarchy of whole-organism phenotypic traits. Funct Ecol 32:958–969;
855 doi:10.1111/1365-2435.13033.

856 Meserve JH, Nelson JC, Marsden KC, Hsu J, Echeverry FA, Jain A, et al. 2020. A forward
857 genetic screen identifies Dolk as a regulator of startle magnitude through the potassium
858 channel subunit Kv1.1. bioRxiv.

859 Meyers JR, MacDonald RB, Duggan A, Lenzi D, Standaert DG, Corwin JT, et al. 2003.
860 Lighting up the senses: FM1-43 loading of sensory cells through nonselective ion
861 channels. J Neurosci 23:4054–65; doi:10.1523/JNEUROSCI.23-10-04054.2003.

862 Nakayama H. 2004. Common sensory inputs and differential excitability of segmentally
863 homologous reticulospinal neurons in the hindbrain. J Neurosci 24:3199–3209;

doi:10.1523/JNEUROSCI.4419-03.2004.

Nyffeler J, Chovancova P, Dolde X, Holzer AK, Purvanov V, Kindinger I, et al. 2018. A structure–activity relationship linking non-planar PCBs to functional deficits of neural crest cells: new roles for connexins. Arch Toxicol 92:1225–1247; doi:10.1007/s00204-017-2125-4.

Oikonomou G, Altermatt M, Zhang R wei, Coughlin GM, Montz C, Gradinaru V, et al. 2019. The serotonergic raphe promote sleep in zebrafish and mice. Neuron 103:686-701.e8; doi:10.1016/j.neuron.2019.05.038.

Panlilio JM, Aluru N, Hahn ME. 2020. Developmental neurotoxicity of the harmful algal bloom toxin domoic acid: Cellular and molecular mechanisms underlying altered behavior in the zebrafish Model. Environ Health Perspect 128:117002; doi:10.1289/EHP6652.

Panlilio JM, Jones IT, Salanga MC, Aluru N, Hahn ME. 2021. Developmental exposure to domoic acid disrupts startle response behavior and circuitry. bioRxiv; doi:10.1101/2021.01.08.425996.

Park H-C, Shin J, Roberts RK, Appel B. 2007. An olig2 reporter gene marks oligodendrocyte precursors in the postembryonic spinal cord of zebrafish. Dev Dyn 236:3402–3407; doi:10.1002/dvdy.21365.

Patel JF, Hartman TJ, Sjodin A, Northstone K, Taylor E V. 2018. Prenatal exposure to polychlorinated biphenyls and fetal growth in British girls. Environ Int 116:116–121; doi:10.1016/j.envint.2018.04.007.

Poon E, Bandara SB, Allen JB, Sadowski RN, Schantz SL. 2015. Developmental PCB exposure increases susceptibility to audiogenic seizures in adulthood. Neurotoxicology 46:117–124; doi:10.1016/j.neuro.2014.12.007.

Pruitt DL, Meserve LA, Bingman VP. 1999. Reduced growth of intra- and infra-pyramidal mossy fibers is produced by continuous exposure to polychlorinated biphenyl. Toxicology 138:11–17; doi:10.1016/S0300-483X(99)00073-6.

Pujol-Martí J, López-Schier H. 2013. Developmental and architectural principles of the lateral-line neural map. Front Neural Circuits 7:47; doi:10.3389/fncir.2013.00047.

Ranasinghe P, Thorn RJ, Seto R, Creton R, Bridges WC, Chapman SC, et al. 2019. Embryonic exposure to 2,2′,3,5′,6-pentachlorobiphenyl (PCB-95) causes developmental malformations in zebrafish. Environ Toxicol Chem 39:162–170; doi:10.1002/etc.4587.

Ribas-Fitó N, Sala M, Kogevinas M, Sunyer J. 2001. Polychlorinated biphenyls (PCBs) and neurological development in children: A systematic review. J Epidemiol Community Health 55:537–546; doi:10.1136/jech.55.8.537.

Rice D, Barone S. 2000. Critical periods of vulnerability for the developing nervous system: Evidence from humans and animal models. Environ Health Perspect 108:511–533; doi:10.2307/3454543.

Roberts A. 2000. Early functional organization of spinal neurons in developing lower vertebrates. Brain Res Bull 53:585–593; doi:10.1016/S0361-9230(00)00392-0.

904 Rungta RL, Choi HB, Tyson JR, Malik A, Dissing-Olesen L, Lin PJC, et al. 2015. The cellular
905 mechanisms of neuronal swelling underlying cytotoxic edema. Cell 161:610–621;
906 doi:10.1016/j.cell.2015.03.029.

907 Schindelin J, Arganda-Carreras I, Frise E, Kaynig V, Longair M, Pietzsch T, et al. 2012. Fiji:
908 An open-source platform for biological-image analysis. Nat Methods 9:676–682;
909 doi:10.1038/nmeth.2019.

910 Seegal RF, Bush B, Shain W. 1990. Lightly chlorinated ortho-substituted PCB congeners
911 decrease dopamine in nonhuman primate brain and in tissue culture. Toxicol Appl
912 Pharmacol 106: 136–44.

913 Serrano-Velez JL, Rodriguez-Alvarado M, Torres-Vazquez II, Fraser SE, Yasumura T,
914 Vanderpool KG, et al. 2014. Abundance of gap junctions at glutamatergic mixed
915 synapses in adult Mosquitofish spinal cord neurons. Front Neural Circuits 8:66;
916 doi:10.3389/fncir.2014.00066.

917 Shin J, Park H-C, Topczewska JM, Mawdsley DJ, Appel B. 2003. Neural cell fate analysis in
918 zebrafish using <i>olig2<i> BAC transgenics. Methods Cell Sci 25:7–14;
919 doi:10.1023/B:MICS.0000006847.09037.3a.

920 Smith NL, Kimelman D. 2019. *Establishing the body plan: The first 24 hours of zebrafish*
921 *development*. Elsevier.

922 Stenberg M, Hamers T, Machala M, Fonnum F, Stenius U, Lauy AA, et al. 2011. Multivariate
923 toxicity profiles and QSAR modeling of non-dioxin-like PCBs - An investigation of in vitro
924 screening data from ultra-pure congeners. Chemosphere 85:1423–1429;
925 doi:10.1016/j.chemosphere.2011.08.019.

926 Stewart AM, Braubach O, Spitsbergen J, Gerlai R, Kalueff A V. 2014. Zebrafish models for
927 translational neuroscience research: From tank to bedside. Trends Neurosci 37:264–
928 278; doi:10.1016/j.tins.2014.02.011.

929 Ta TA, Feng W, Molinski TF, Pessah IN. 2006. Hydroxylated xestospongins block inositol-
930 1,4,5-trisphosphate-induced Ca^{2+} release and sensitize Ca^{2+}-induced Ca^{2+} release
931 mediated by ryanodine receptors. Mol Pharmacol 69:532–538;
932 doi:10.1124/mol.105.019125.used.

933 Tabor KM, Bergeron SA, Horstick EJ, Jordan DC, Aho V, Porkka-Heiskanen T, et al. 2014.
934 Direct activation of the Mauthner cell by electric field pulses drives ultrarapid escape
935 responses. J Neurophysiol 112:834–844; doi:10.1152/jn.00228.2014.

936 Takada N, Kucenas S, Appel B. 2010. Sox10 is necessary for oligodendrocyte survival
937 following axon wrapping. Glia 58:996–1006; doi:10.1002/glia.20981.

938 Tanaka Y, Fujiwara M, Shindo A, Yin G, Kitazawa T, Teraoka H. 2018. Aroclor 1254 and
939 BDE-47 inhibit dopaminergic function manifesting as changes in locomotion behaviors
940 in zebrafish embryos. Chemosphere 193:1207–1215;
941 doi:10.1016/j.chemosphere.2017.11.138.

942 Toro C, Trapani JG, Pacentine I, Maeda R, Sheets L, Mo W, et al. 2015. Dopamine
943 modulates the activity of sensory hair cells. J Neurosci 35:16494–16503;
944 doi:10.1523/JNEUROSCI.1691-15.2015.

945 Trnovec T, Šovčíková E, Pavlovčinová G, Jakubíková J, Jusko TA, Husťák M, et al. 2010.
946 Serum PCB concentrations and cochlear function in 12-year-old children. Environ Sci
947 Technol 44:2884–2889; doi:10.1021/es901918h.

948 Troconis EL, Ordoobadi AJ, Sommers TF, Aziz-Bose R, Carter AR, Trapani JG. 2017.
949 Intensity-dependent timing and precision of startle response latency in larval zebrafish.
950 J Physiol 595:265–282; doi:10.1113/JP272466.

951 Tropepe V, Sive HL. 2003. Can zebrafish be used as a model to study the
952 neurodevelopmental causes of autism? Genes, Brain Behav 2:268–281;
953 doi:10.1034/j.1601-183X.2003.00038.x.

954 Vettori MV, Goldoni M, Caglieri A, Poli D, Folesani G, Ceccatelli S, et al. 2006. Antagonistic
955 effects of methyl-mercury and PCB153 on PC12 cells after a combined and
956 simultaneous exposure. Food Chem Toxicol 44:1505–1512;
957 doi:10.1016/j.fct.2006.04.009.

958 Voesenek CJ, Muijres FT, Van Leeuwen JL. 2018. Biomechanics of swimming in developing
959 larval fish. J Exp Biol 221; doi:10.1242/jeb.149583.

960 Walkowiak J, Wiener J-A, Fastabend A, Heinzow B, Krämer U, Schmidt E, et al. 2001.
961 Environmental exposure to polychlorinated biphenyls and quality of the home
962 environment: effects on psychodevelopment in early childhood. Lancet 358:1602–1607;
963 doi:10.1016/S0140-6736(01)06654-5.

964 Wigestrand MB, Stenberg M, Walaas SI, Fonnum F, Andersson PL. 2013. Non-dioxin-like
965 PCBs inhibit [3H]WIN-35,428 binding to the dopamine transporter: A structure–activity
966 relationship study. Neurotoxicology 39:18–24; doi:10.1016/J.NEURO.2013.07.005.

967 Wolman MAA, Jain RAA, Marsden KCC, Bell H, Skinner J, Hayer KEE, et al. 2015. A
968 genome-wide screen identifies PAPP-AA-mediated IGFR signaling as a novel regulator
969 of habituation learning. Neuron 85:1200–1211; doi:10.1016/j.neuron.2015.02.025.

970 Yang D, Kim KH, Phimister A, Bachstetter AD, Ward TR, Stackman RW, et al. 2009.
971 Developmental exposure to polychlorinated biphenyls interferes with experience-
972 dependent dendritic plasticity and ryanodine receptor expression in weanling rats.
973 Environ Health Perspect 117:426–435; doi:10.1289/ehp.11771.

974 Zhao Y, Liang J, Meng H, Yin Y, Zhen H, Zheng X, et al. 2020. Rare earth elements
975 lanthanum and praseodymium adversely affect neural and cardiovascular development
976 in zebrafish (Danio rerio). Environ Sci Technol; doi:10.1021/acs.est.0c06632.

977 **Figures**

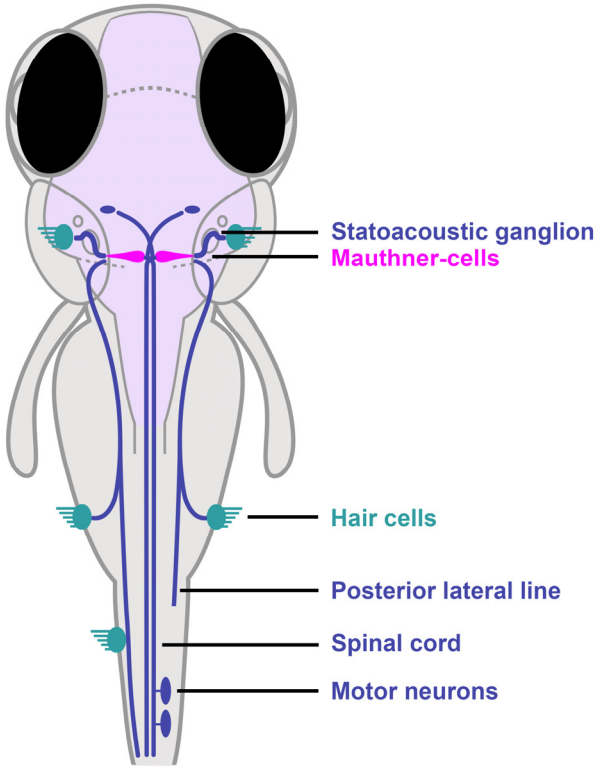

978

979 **Figure 1. Startle response circuit in zebrafish.** The proper execution of the auditory-evoked
980 startle response relies on hair cells to sense the auditory stimulus, Mauthner-cells to integrate
981 the signals, and motor neurons and musculature to execute the startle behavior.

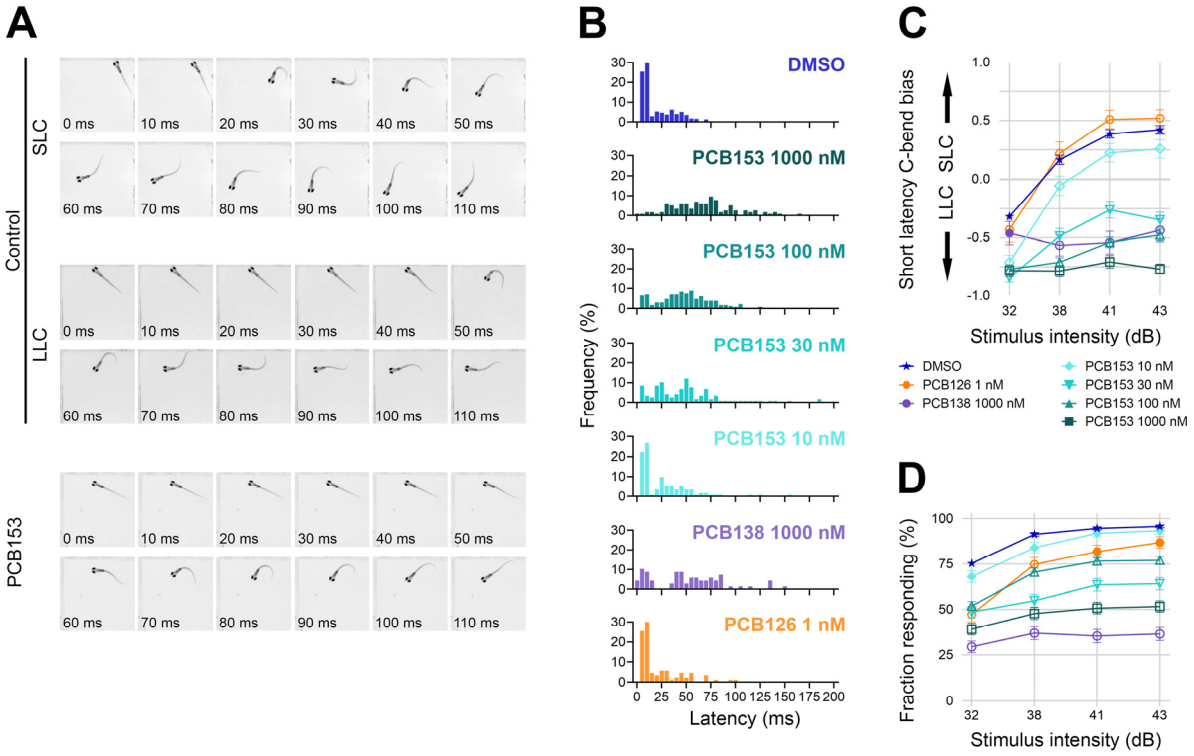

Figure 2. Effect of PCBs on startle response in 6 dpf zebrafish. (**A**) Representative short-latency C-bend (SLC) and long-latency C-bend (LLC) startle response of a control zebrafish larva at 6 dpf in comparison to a typical response of a PCB153 treated larva. (**B**) Vibro-acoustic startle latency at highest stimulus intensity (43 dB) in vehicle control (n = 479), NDL PCB153 1000 nM (n = 179), NDL PCB153 100 nM (n = 253), NDL PCB153 30 nM (n = 152), NDL PCB153 10 nM (n = 119), NDL PCB138 (n = 139), and DL PCB126 (n = 97) exposed larvae. (**C**) Bias of SLC and LLC and (**D**) response rate of different exposure groups at different vibro-acoustic intensities. Values are presented as mean ± SEM. All data points are biologically independent replicates from at least three independent experiments. Significant differences to DMSO controls ($p < 0.01$) are indicated by open symbols

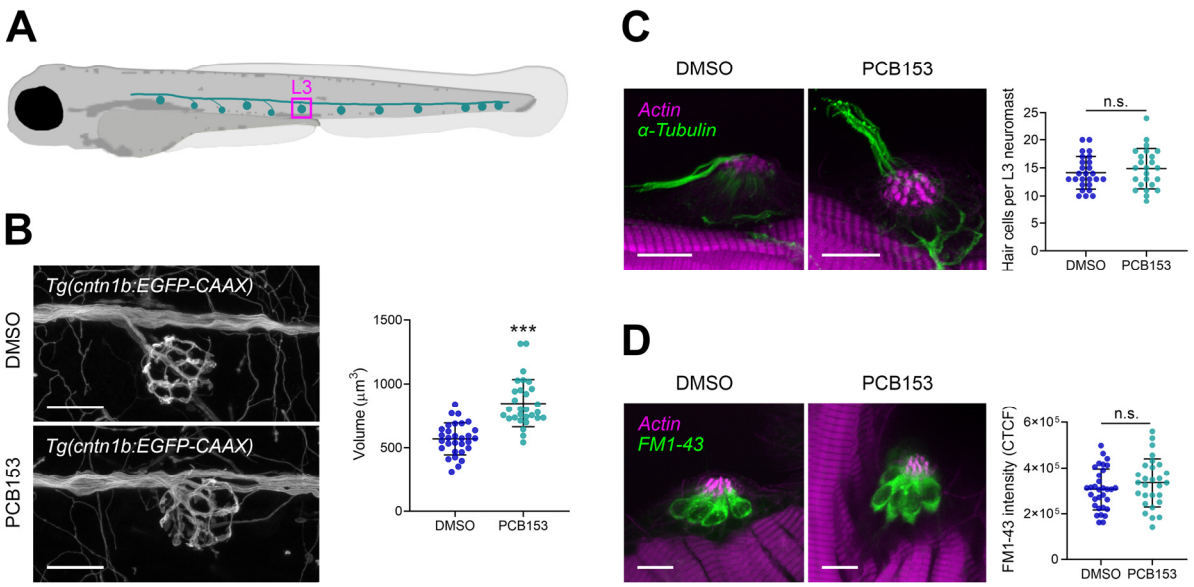

Figure 3. Effect of PCB153 on morphology and function of lateral line hair cells and innervating neurons. (**A**) Diagram indicating L3 neuromast. (**B**) Hair cell innervating neurons at neuromast L3 shown using *Tg(cntn1b:EGFP-CAAX)*. Volume of hair cell innervating neurons of DMSO (n = 30) and PCB153 (n = 29) treated larvae. Scale bar = 20 µm. (**C**) Whole-mount immune staining of kinocilia and hair cell innervating neurons (anti-acetylated tubulin antibody; green) and counterstain of stereocilia bundles and muscle tissue (actin; magenta) of DMSO (n = 26) and PCB153 (n = 24) treated larvae. The hair cell number was determined based on the number of kinocilia. Scale bar = 10 µm (**D**) Uptake of FM-143 dye as indication of functional hair cells of DMSO (n = 32) and PCB153 (n = 28) treated larvae. Scale bar = 10 µm. All data points are biologically independent replicates from three independent experiments. Asterisks indicate significant differences to controls (***$p < 0.001$).

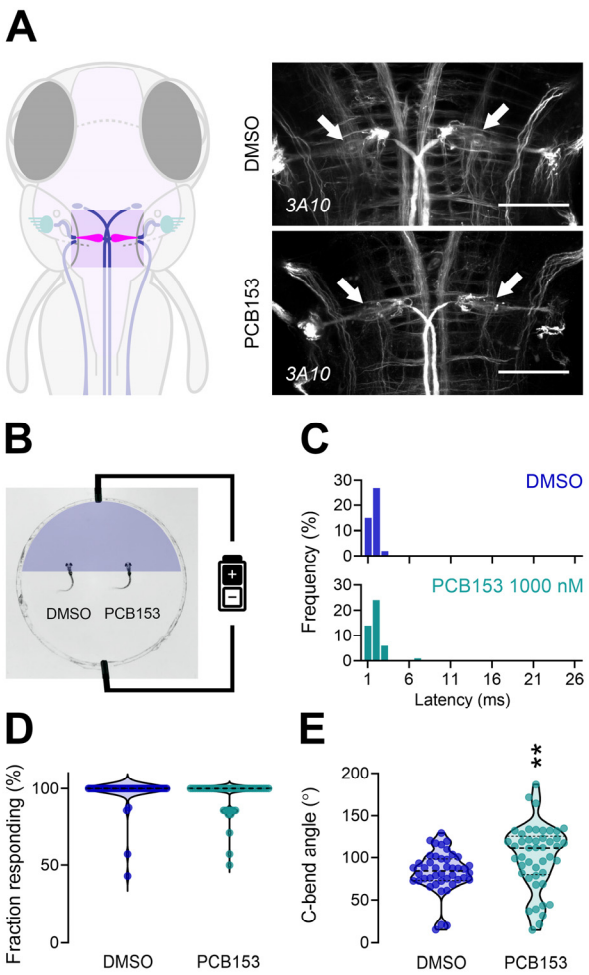

Figure 4. Effect of PCB153 on morphology and function of the Mauthner-cells. (**A**) Diagram indicating localization of Mauthner-cells in the hindbrain and brain tissue immunostaining with anti-neurofilament 3A10 antibody labeling reticulospinal neurons in control and PCB153 treated larvae at 6 dpf (ventral view). Mauthner (arrow) cells were present in all brain tissues (control: n = 23, PCB153: n = 21). Scale bar = 50 µm. (**B**) Diagram of electrical stimulation performed to assess the functionality of Mauthner-cells. Both DMSO (n = 44) and PCB153 (n = 45) treated larvae show similar (**C**) latency to electrical stimulation and (**D**) response frequency (seven stimuli per larvae), indicating that the M-cells are present and functional. (**E**) The increased C-bend angle in PCB153 exposed larvae may be indicative of impaired motoneuron or muscle development. All data points are biologically independent replicates (one value representing the mean of seven consecutive electric field pulses) from three independent experiments. Dashed lines represent median and quartiles and asterisks indicate significant differences to controls (**$p < 0.01$).

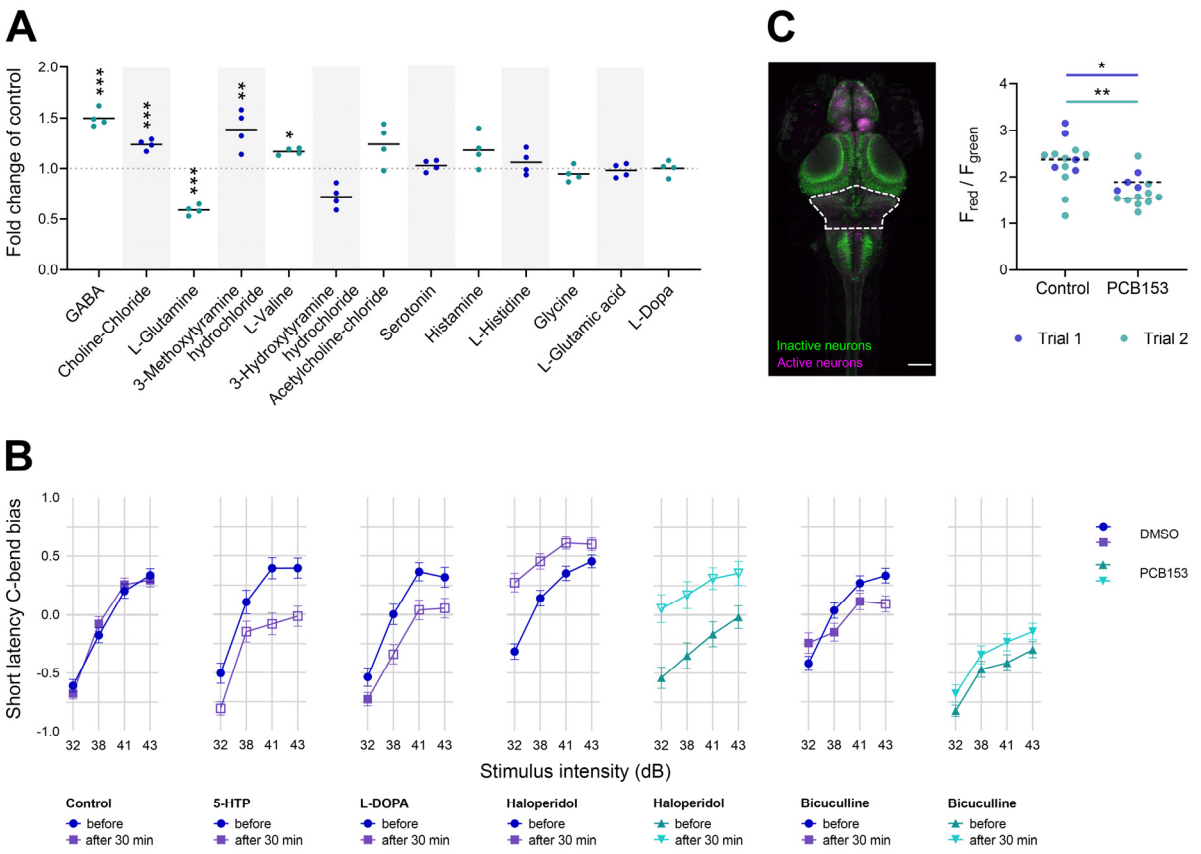

Figure 5. Involvement of neurotransmitters in startle latency. (**A**) Neurotransmitter levels in 6 dpf larvae exposed to 1000 nM PCB153 in comparison to control (*n* = 4). (**B**) Startle bias shift induced by 30-minute exposure to serotonin, dopamine, and GABA neurotransmitter modulators in 6 dpf control and 100 nM PCB153 exposed larvae. Control (*n* = 138-172), 5-HTP (*n* = 67-80), L-DOPA (*n* = 76-94), haloperidol (Control *n* = 123-162, PCB153 *n* = 37-61), and bicuculline (Control *n* = 90-162, PCB153 *n* = 83-137). All data points are biologically independent replicates from at least three independent experiments. Significant differences to respective controls ($p < 0.01$) are indicated by open symbols. (**C**) Representative maximum intensity z-projection from confocal stack after photoconversions of freely swimming 6 dpf CaMPARI larvae. Scale bar = 100 µm. Ratio of red to green fluorescence intensity in the rostral hindbrain (indicated by dashed line in image) in DMSO (*n* = 14) and 1000 nM PCB153 (*n* = 14) exposed startling larvae in 4 ˚C (cold) medium. Dashed lines indicate median per trial. Two independent experiments. Asterisks indicate significant differences to controls (*p < 0.05, **p < 0.01, and ***p < 0.001).